

We are IntechOpen, the world's leading publisher of Open Access books Built by scientists, for scientists

4,800

Open access books available

122,000

International authors and editors

135M

Downloads

Our authors are among the

154

Countries delivered to

TOP 1%

most cited scientists

12.2%

Contributors from top 500 universities

**WEB OF SCIENCE™**Selection of our books indexed in the Book Citation Index
in Web of Science™ Core Collection (BKCI)

Interested in publishing with us?
Contact book.department@intechopen.com

Numbers displayed above are based on latest data collected.

For more information visit www.intechopen.com

Norland Optical Adhesive 65[®] as Holographic Material

J.C. Ibarra¹, L. Aparicio-Ixta², M. Ortiz-Gutiérrez² and C.R. Michel¹

¹CUCEI, Universidad de Guadalajara

²Universidad Michoacana de San Nicolás de Hidalgo
México

1. Introduction

Research on photosensitive materials is an active field where the main goal is to find materials with desirable characteristics for optical data storage. Some of these special characteristics are high sensibility, high resolution and wide spectral range, low cost, among others (Smith, 1975). For this purpose many kinds of materials that for this purpose, such as silver halide, photoresist, dichromated gelatin, photopolymers, thermal recording materials, photothermoplastics, photocromics, and photorefractive crystals (Bjelkhangen & Thompson, 1996; Hariharan, 1980; Kang et al., 2004; Koustuk, 1999) have been used. The most widely used at present are photopolymers.

Photopolymers have excellent holographic characteristics, such as high refraction index modulation, real time recording, low cost, etc. The response on these materials depends of parameters such as incident beam intensity, monomers concentration, polymerization velocity, humidity, temperature, thickness of the sample, etc. (Adhami et al., 1991; Gallego et al., 2005; Gleeson, et al., 2005). Recent papers show that photopolymer's thickness is of great importance (Neipp et al., 2003; Ortuño, et al., 2003). The spectral sensibility of these materials can be easily modified if the photopolymers are mixed with dyes such as crystal violet (Luna et al., 1997,1998; Ortiz et al. 2007).

Some photopolymers employed in optical storage are given in (K. & M. Budinski, 1999; Fernandez et al., 2006; Ibarra & Olivares, 2006; Leclere et al., 1995; Naydenova et al., 2006). One of these polymers is an adhesive called Norland Optical Adhesive 65[®] (NOA 65[®]). (Pinto & Olivares, 2002) and co-workers report that they have used NOA 65[®] in its natural form to record computer generated Fourier holograms using microlithography techniques. Recently (Aleksejeva & Teteris, 2010), the photopolymers NOA 60, NOA 61, NOA 63, NOA 65 and NOA 68 were studied as materials for fabrication of volume gratings, they recorded transmission and reflection diffraction gratings and used a He-Cd laser of 325nm line, obtaining diffraction efficiency >80%.

In this work a study became of the holographic material composed by Norland Optical adhesive 65 (NOA 65) mixed with crystal violet dye (CV) was made. In this material we recorded transmission real time phase holographic gratings and Fourier holograms. obtaining diffraction efficiency of 1.85% using a light beam at wavelength 598 nm from a He-Ne laser was obtained. The gratings were recorded changing parameters such as

concentrations between NOA 65 and CV, sample thickness, beams intensity ratio and spatial frequency. The material shows refraction index modulation, which is calculated using the Kogelnik's theory. The results obtained are show by the behavior of diffraction efficiency versus energy.

2. Materials properties

2.1 Norland Optical Adhesive 65 (NOA 65®)

This polymer is typically used for putting lenses in metal mounts, bounding plastic to glass and cold blocking by cured process. The polymer cure process depends on intensity and wavelength of the UV radiation. Before being exposed to UV radiation, the polymer's adhesive is in liquid state because the monomers and photo initiators will not react with each other. When exposed to UV, the photo initiators undergo a change creating free radicals that react with monomers, producing monomer chains. In the cured state, the monomer chains convert to cross-linked polymer chains.

The absorbance spectra of the NOA 65® obtained with an UV-Vis spectrophotometer is show in Fig. 1, where we can observe that its absorbance displays a plateau in the visible region, showing a maximum absorption in 300 nm. Complementary to this plot, Fig. 2 show the spectral transmission for the UV-Vis-IR regions. The plot was obtained from (Norland Products Incorporate, 1999).

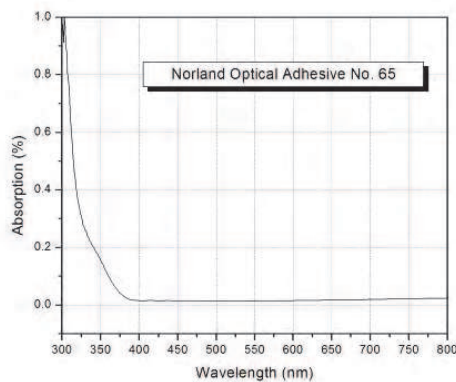


Fig. 1. Absorption spectra of NOA 65 in region UV-Vis.

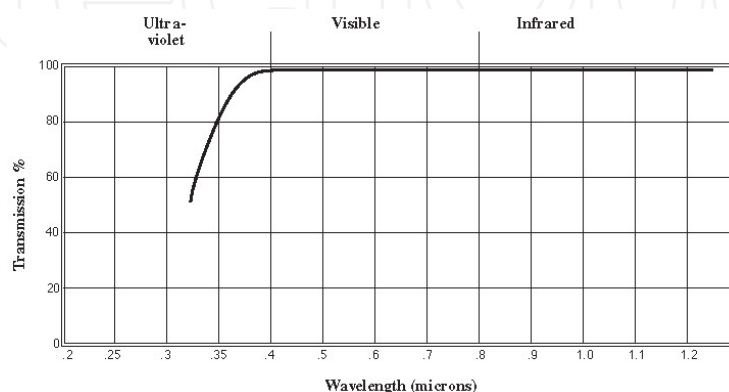


Fig. 2. Transmission spectra for NOA 65.

Table 1 shows some properties of NOA 65 whereas Table 2 shows the typical cure times according to Norland Products instructions.

| | |
|-----------------------------------|------------|
| Solids | 100% |
| Viscosity at 25°C | 1,200 |
| Refractive Index of Cured Polymer | 1.524 |
| Elongation at Failure | 80% |
| Modulus of Elasticity (psi) | 20,000 |
| Tensile Strength (psi) | 1,500 |
| Hardness - Shore D | 50 |
| Temperature Range | -15 to 60° |

Table 1. Typical properties of NOA 65.

| LIGHT SOURCE | FILM THICKNESS | PRECURE | FULL CURE |
|---|----------------|------------|------------|
| 100 Watt Mercury* Spot Lamp at 6 inches | 1-10 mil | 15 seconds | 5 minutes |
| 2-15 Watt Fluorescent* Black Lights at 3 inches | 1-10 mil | 60 seconds | 20 minutes |

Table 2. Typical cure times of NOA 65.

Fig. 3 shows the absorbance spectra obtained with a FTIR spectrophotometer showing absorption peaks, indicating the presence of some compounds Table 3 displays brief analysis of the NOA 65 IR spectrum. briefly analysis of the NOA 65® IR spectrum.

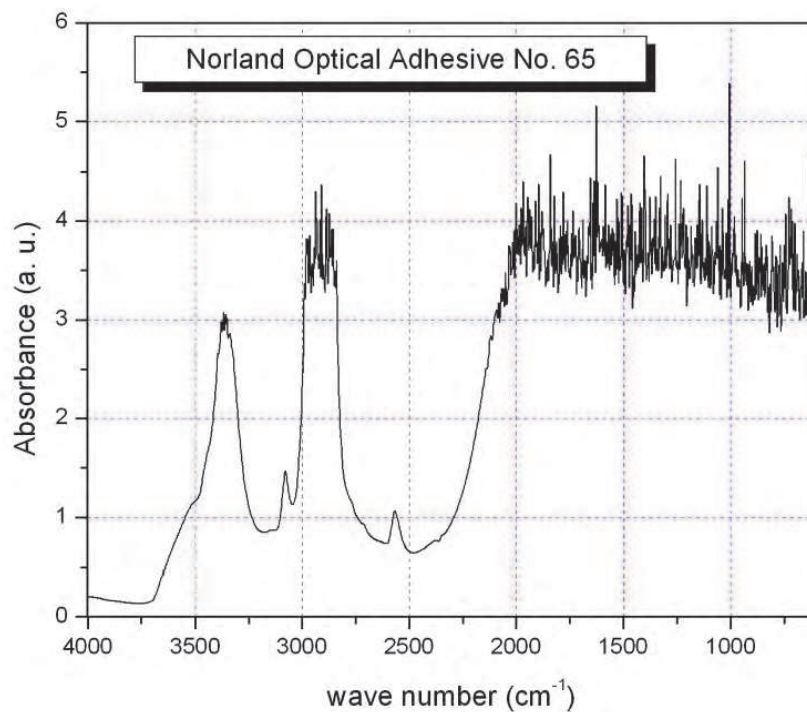


Fig. 3. Absorbance spectra in IR region

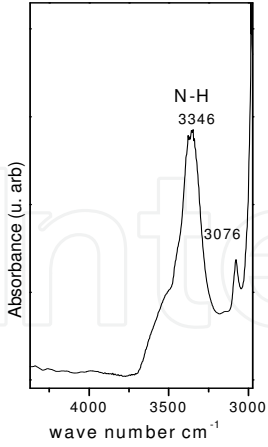
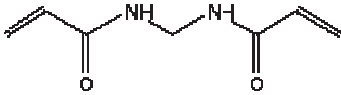
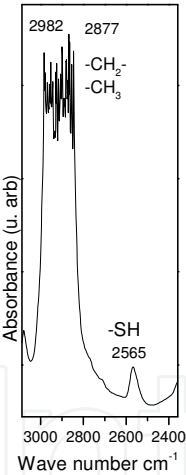

| Wave number | Group | Strain | Note |
|---|---|------------------------------|---|
|  | N-H | Asymmetric vibration | For Secondary amide (NH-CO) not associated, they have a sharp and big band to 3460-3300 cm ⁻¹ Amide in liquid phase, They exhibit a big band to 3270 and a weak band to 3100-3070. |
| | N-H 3346 | Asymmetric vibration | |
| Possible structure |  | | 2-Propenamamide, n,n'-methylenebis Or metilenebisacrylamide. |
|  | CH ₃ - 2982 | Asymmetric vibration 2980 | In 2982-2877 cm ⁻¹ interval appear aliphatic groups CH ₃ and CH ₂ . The vibration that appears to 255 corresponds to the vibration of the SH, reported as more characteristic band of the thiols. A double SH due to the intensity of this band has been considered. |
| | CH ₂ - 2877 | Asymmetric vibration 2900±45 | |
| Possible structure |  | | |

Table 3. IR analysis for NOA 65.

2.2 Crystal violet dye

The crystal violet dye (CV) is a dark green powder soluble in water, chloroform, isopropyl alcohol, but not in ether and ethylic alcohol. The crystal violet dye can be used as antiseptic and a pH indicator for some substances. Its chemical composition is $C_{25}H_{30}ClN_3$ and molecular weight 407.98. In Fig 4 we show its absorption spectra showing a peak in the spectral line at 591 nm, making a displacement of the absorption curve towards the yellow and orange color

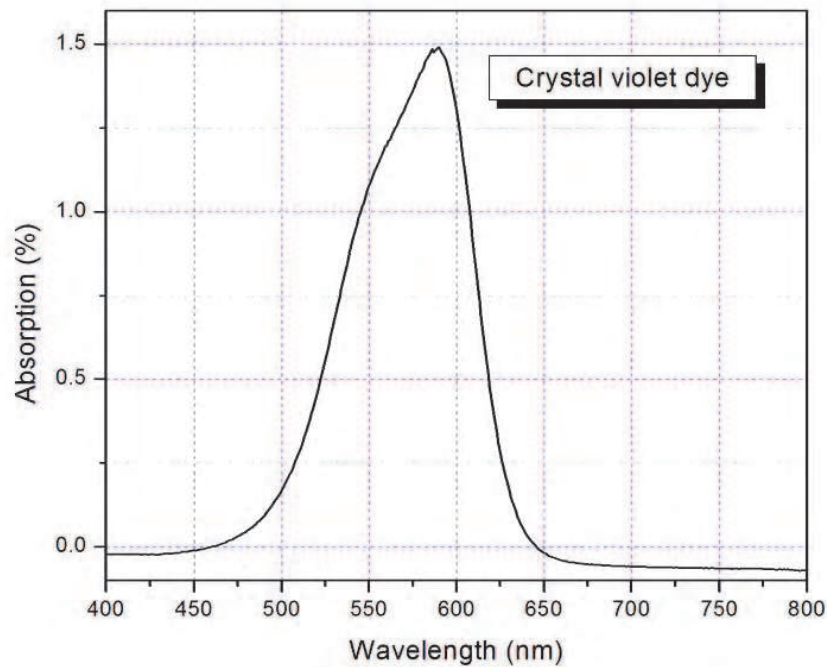


Fig. 4. Absorbance spectra of CV dye showing a peak at 580 nm.

2.3 Photosensitive material

The mix of NOA 65[®] and CV dye composed the photosensitive material. We prepare three different concentrations varying the quantities of the NOA 65[®] and CV as mentioned in Table 4 when the compounds are mixed, we deposit them into different glass cells fabricated with two glass substrates separated by mylar (17 μm thickness), cellophane (27 μm thickness) or mica (110 μ thickness), All the thicknesses used in this work were measured with an electronic micrometer. The mixture was introduced into the cell by the gravity technique as is shown in Fig. 5

| Concentration | NOA 65 [®] | CV |
|----------------|---------------------|--------|
| C ₁ | 99.95 % | 0.05 % |
| C ₂ | 99.9 % | 0.1 % |
| C ₃ | 99.85 % | 0.15 % |

Table 4. Relation of concentration between NOA 65 and CV.

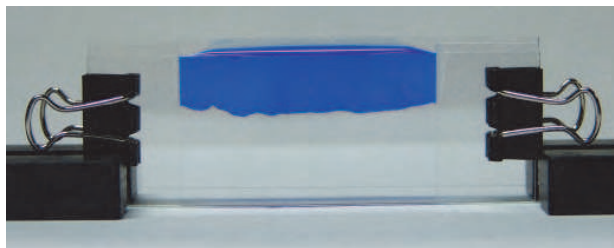


Fig. 5. Photography of the emulsion between two glasses deposited by gravity technique.

Fig. 6 show the absorption spectra in the UV-Vis region of the photosensitive film. The curves correspond to the three concentrations that we prepare and all the concentrations have absorption located in 500 – 630 nm range with a peak in the spectral line at 591 nm.

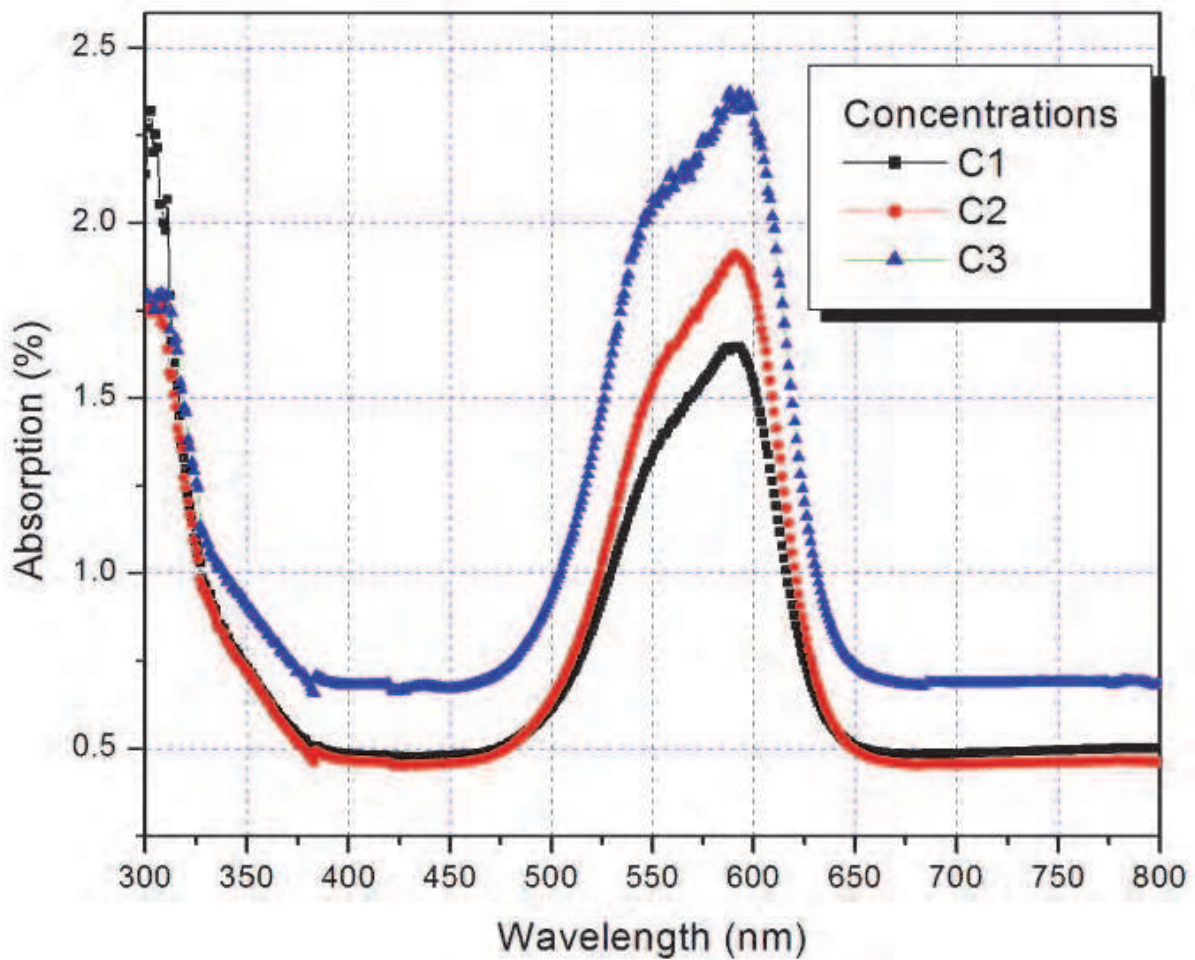


Fig. 6. Absorption spectra of mix NOA 65 and CV for three concentrations of 110 μm thickness cell.

In Table 5 we show the absorption coefficients for the 110 μm thickness sample obtained with the Beer's law considering the spectrum of Fig. 5. In eq. 1 we write the absorption A , as function of the molar concentration c , thickness l , and the absorption coefficient α .

$$A = cl\alpha \quad (1)$$

| Concentration | l (μm) | α ($\lambda=598$ nm) | α ($\lambda=543$ nm) |
|----------------|-----------------------|------------------------------|------------------------------|
| C ₁ | 110 | 0.004201745 | 0.001964058 |
| C ₂ | 110 | 0.005589304 | 0.003213745 |
| C ₃ | 110 | 0.00773117 | 0.006168739 |

Table 5. Absorption coefficient for the mix NOA 65 and CV.

3. Experimental process

To record the phase holographic gratings in the photosensitive material we use the experimental setup shown in Fig. 7. We use a beam from a He-Ne laser with emission line at $\lambda=598$ nm corresponding to yellow color which is separated into two beams by a beam splitter (BS). The beams are reflected by two mirrors (M_1 and M_2) toward the photosensitive material (PM) where an interference pattern is formed and recorded in real time by the period of 3 hours continuous.

In order to realize the measurements of the diffraction efficiency of the holographic grating we use a He-Ne laser as reading beam with emission line at $\lambda=545$ nm, which corresponds to green color, it is because this line does not affect the grating's recording process. The gratings we record in this photosensitive material correspond to phase holographic gratings by refraction index modulation.

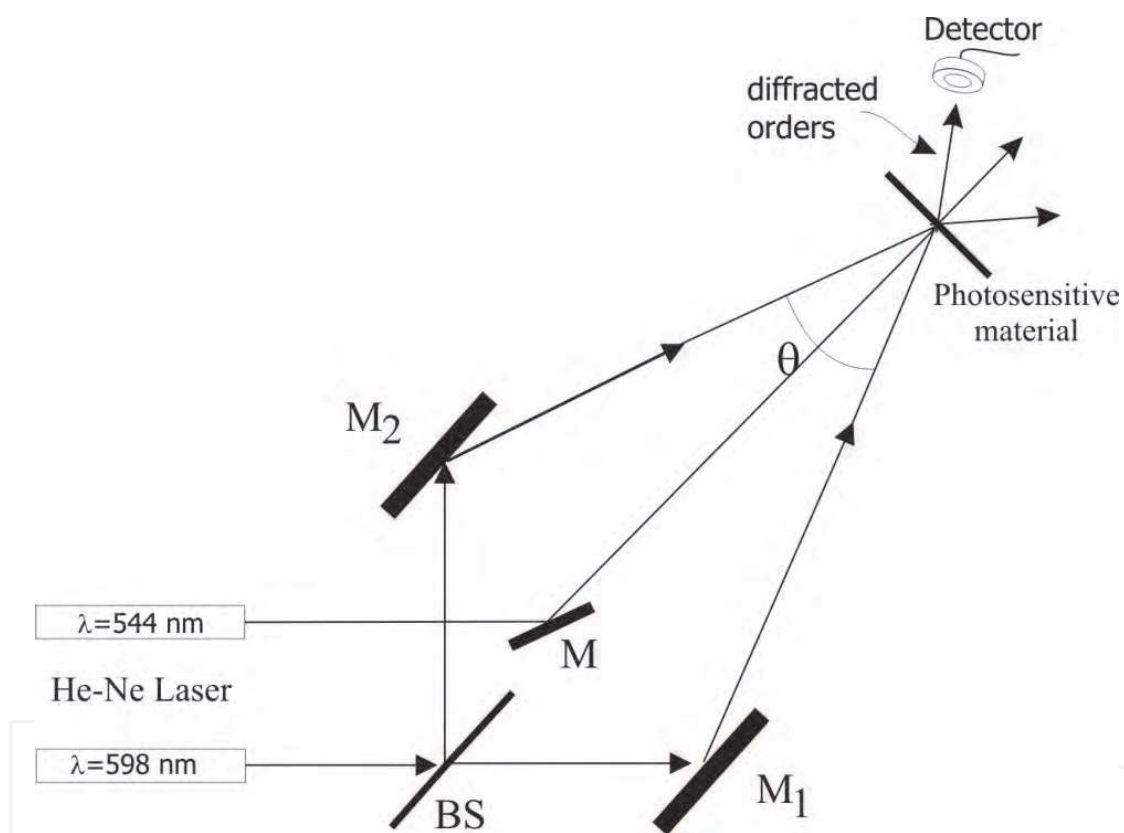


Fig. 7. Setup to make diffraction grating in real time.

The diffraction efficiency is defined as +1 diffracted order intensity and incident beam intensity ratio expressed as percentage as is represented in eq. 2.

$$\eta(\%) = \frac{I_1}{I_i} \times 100 \quad (2)$$

Where I_1 is the +1 diffracted order intensity and I_i the incident beam intensity. This equation is not considering the Fresnel losses because of the reflection in the photosensitive cell.

The Fig. 8 is a photography of the diffracted pattern produced by the grating recorded on the material with concentration C3, 110 μm thickness sample, an interference angle of 5 degrees

between the beams which according to Bragg Law produces a grating with spatial frequency of 146 *lines/mm* (the spatial frequency of the gratings is defined as the inverse of the period and is measured as lines per millimeter *lines/mm*). The central spot is called zero diffracted order, inside spots are called -1 and +1 diffracted orders (left and right respectively) and outside spots are -2 and +2 diffracted orders (again left and right spots respectively).

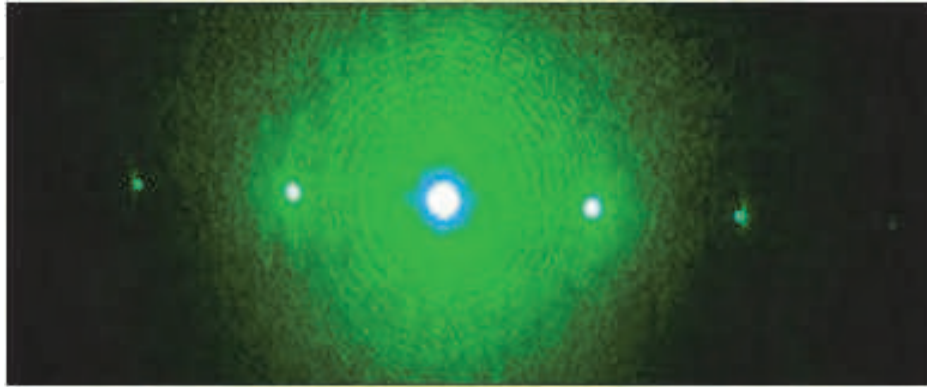


Fig. 8. Real time diffraction pattern showing first and second orders.

3.1 Diffraction gratings in real time

We recorded phase holographic gratings in all material concentrations and thickness and measured the diffraction efficiency. The Fig. 9 shows the diffraction efficiency of the holographic gratings recorded in the 17 μm thickness sample with all concentrations. The diffraction efficiency measurements were taken each 10 minutes after the exposition began. The curves show an increase of the diffraction efficiency concerning exposure energy obtaining $\eta=0.53\%$ as maximum for the concentration C3 (see table 4). These measurements were taken in real time for the +1 diffraction order only.

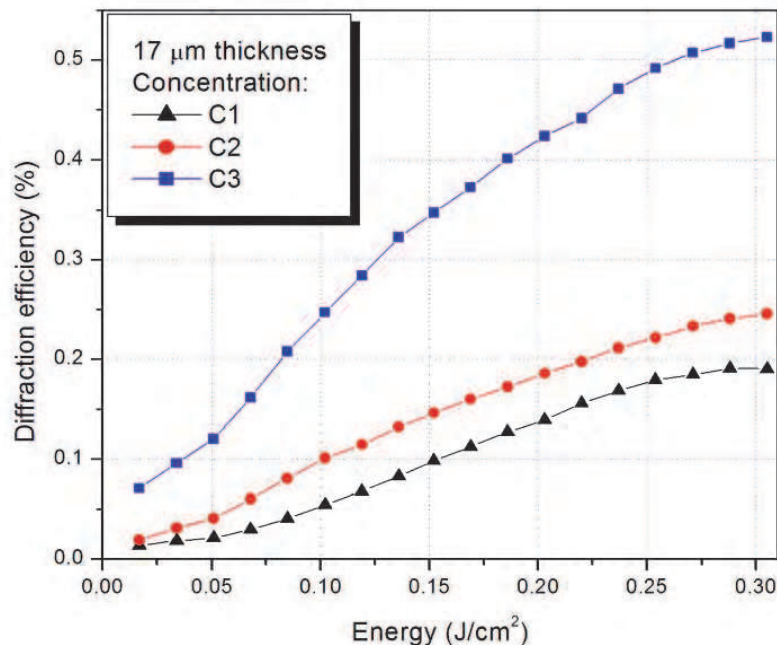


Fig. 9. Diffraction efficiency vs. energy of the three concentrations.

In Fig. 10 we show the diffraction efficiency obtained for all the concentrations again and 27 μm of sample thickness. The maximum diffraction efficiency is for the concentration C3 and its value is 1.1%.

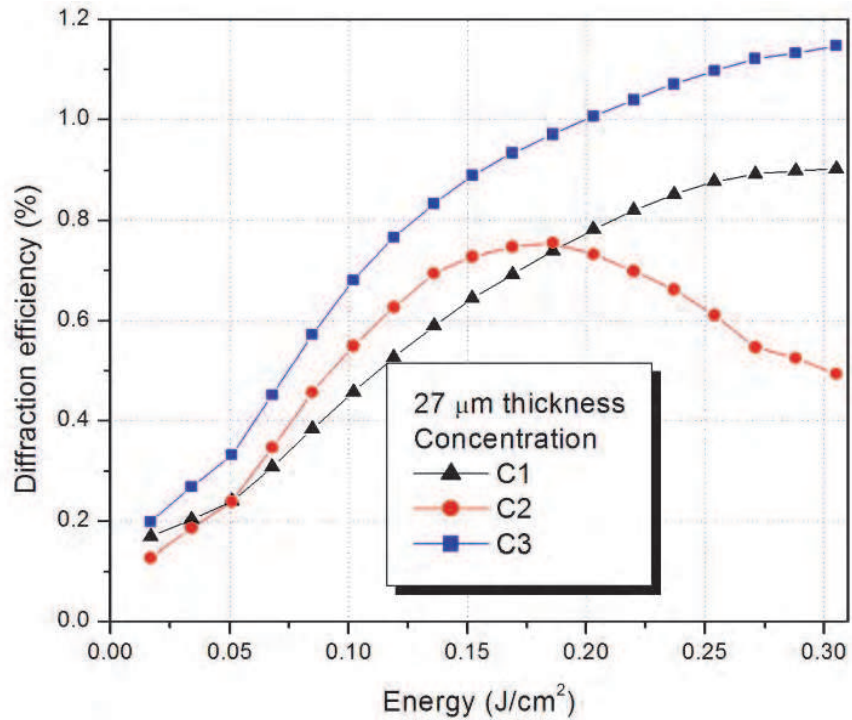


Fig. 10. Diffraction efficiency for the three concentrations and 27 μm sample thickness

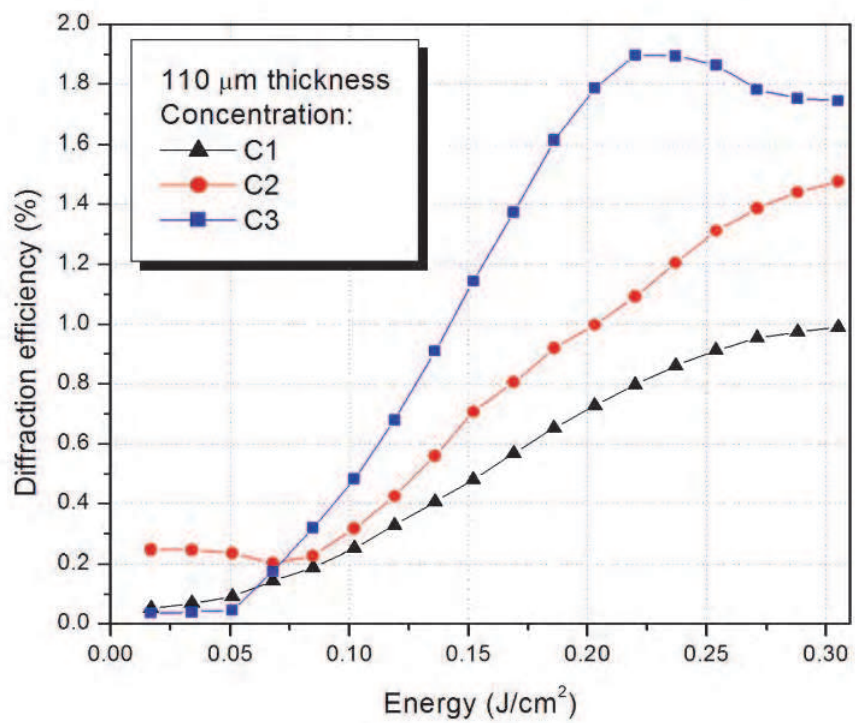


Fig. 11. Diffraction efficiency for the three concentrations, C3 show a major efficiency.

The Fig. 11 shows the results obtained for the 110 μm thickness sample and all the concentrations. Again we record the different gratings in the same conditions. The maximum diffraction efficiency is $\eta=1.85\%$ obtained at 0.225 J/cm^2 using the concentration C3.

It can be observed in the Figs. 9-11, the thickness of the emulsion plays an important role for the grating modulation. We find that the sample of the thickness of 110 μm is adapted to do diffraction gratings because it presents the highest values of diffraction efficiencies.

Another important parameter for the diffraction gratings recorder is the spatial frequency, which can be modified if we change the interference angle between the beams in the setup shown in Fig. 7 this change allows us to obtain gratings with different period according to the Bragg's law.

In this sense, we change the interference angle between the two beams and record holographic gratings in the 110 microns thickness sample using the concentration C3. The angles were fixed at 5, 10 and 15 degrees and the results are shown in Fig. 12. The higher diffraction efficiencies are obtained when the interference angle between the beams is 5° producing a grating with frequency of 146 *lines/mm* and has a value $\eta=1.85\%$. For the 10 and 15 degrees interference angle the diffraction efficiency is very low and produce gratings with 292 *lines/mm* and 436 *lines/mm* respectively. These results suggest us that the material is of low resolution.

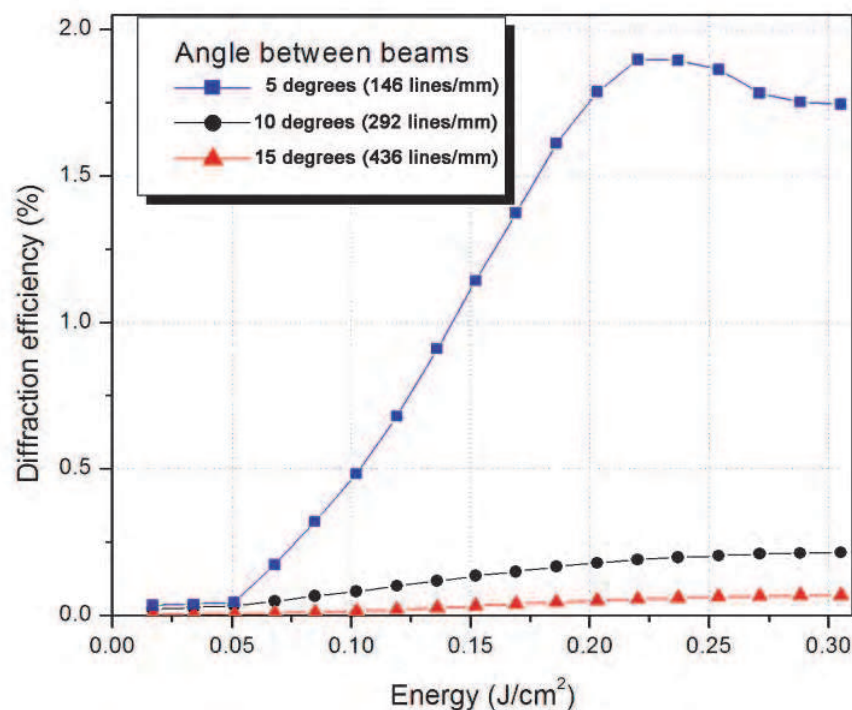


Fig. 12. Diffraction efficiencies for different frequencies.

Finally, we record gratings in the 110 microns thickness sample using the concentration C3 and the interference angle fixed at 5 degrees but we change the beams intensity ratio using the 1:1, 2:1 and 3:1 relations. In Fig. 13 we plot the diffraction efficiency obtained and, as we can see, the diffraction efficiency for the relation 3:1 and 2:1 are very low. The best choices to record holographic gratings in the proposed material are the 110 microns thickness sample prepared with the concentration C3, 5 degrees between the beams and the intensity ratio 1:1.

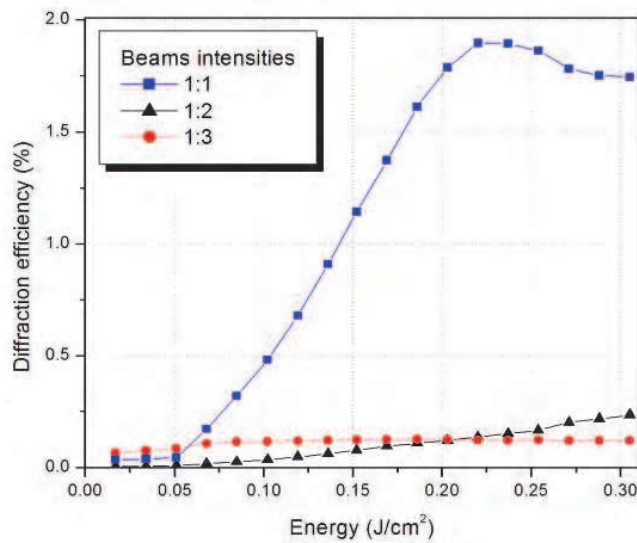


Fig. 13. Diffraction efficiency in function beams intensities ratio. The best diffraction efficiency is obtained at 1:1 relation.

Based on the measured values of the diffraction efficiency η (%) the modulation amplitude of the refraction index Δn can be calculated using the Kogelnik's theory according to the next equation:

$$\Delta n = \frac{\lambda \cos \theta \arcsin \sqrt{\eta}}{\pi d} \tag{3}$$

Where d is the grating's thickness, λ is the reading beam wavelength (in this case $\lambda = 545$ nm) and θ is the incident angle of the reading beam ($\theta=0$) in this case. The Fig. 14 shows the modulation amplitude of the refraction index for three thicknesses of the photosensitive material composed by Norland Optical Adhesive 65® (NOA 65®) mixed with crystal violet dye (CV).

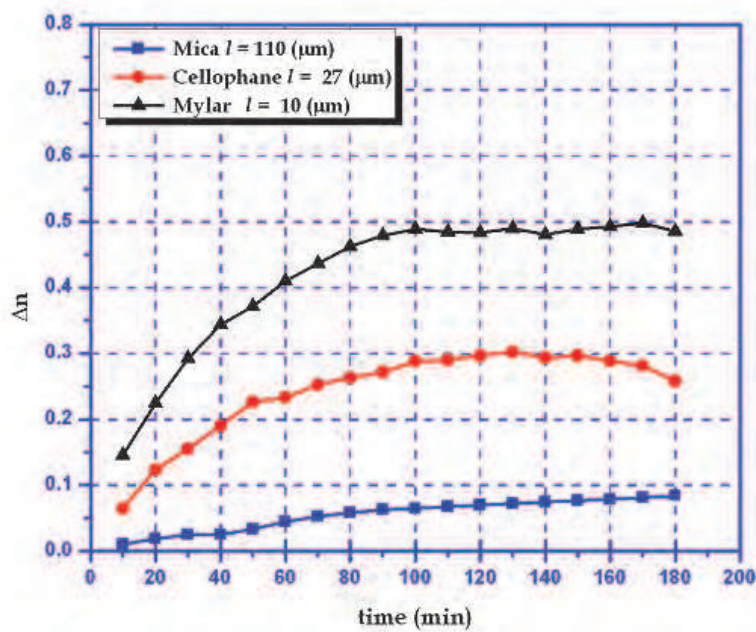


Fig. 14. Modulation amplitude for the refraction index for all thicknesses.

4. The temperature as recording parameter

The diffraction efficiency behavior of the holographic gratings recorded in photopolymers is due to several conditions such as monomer concentration, humidity, temperature, recorder beam intensity, polymerization velocity, mechanical vibrations, etc.

The temperature has an important role during the recording process in our photosensitive material as is shown below. When the material is exposed to interference pattern along 3 hours in small room temperature changes. We measured the temperature each 10 minutes in the photosensitive cell neighborhood and the diffraction efficiency at same time and the results are shown in Fig. 15 we prepare two cells to achieve this proof, so, the red line of the DE in Fig 15(a) corresponds a grating recorded while the room temperature has the behavior showed by red line in Fig. 15(b), using different cell, we record a new grating showing a DE behavior as is indicated by black line in Fig 15(a) while the room temperature has the behavior showed by black line in Fig. 15(b), we repeat this proof for 110 μm , 27 μm and 17 μm thickness cells using the C3 concentration.

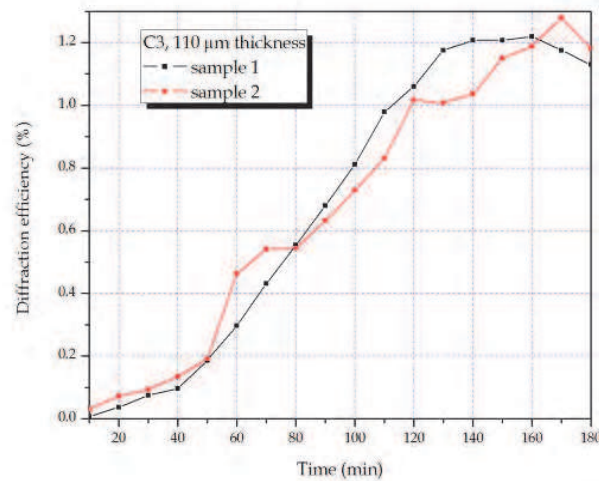


Fig. 15. (a). Diffraction efficiency to certain temperature during the recording process.

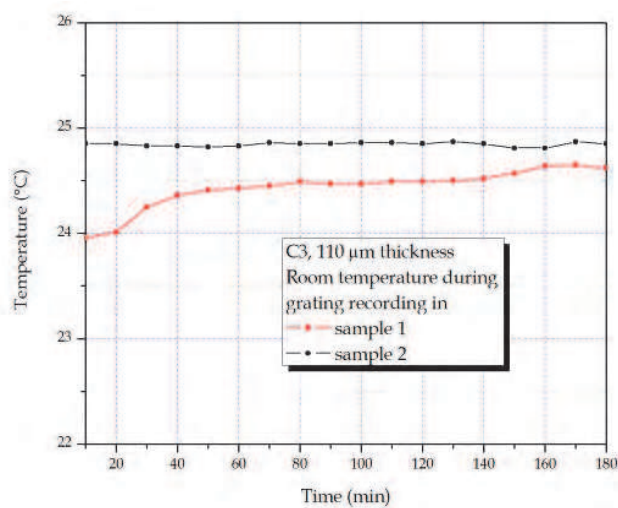


Fig. 15. (b). State of the temperature during the recording process.

Fig. 15 shows the diffraction efficiency and the room temperature during 3 hours. As can be seen, the temperatures have the same behavior and are 25 °C approximately, the DE has a similar values but temperature fluctuations modifies it behavior. When the temperature is almost constant the DE has a softly grow, but when the temperature has some change, the DE show an anomalous behavior. The same behavior for 27 μm and 17 μm was observed as is shown in Fig. 16 and 17.

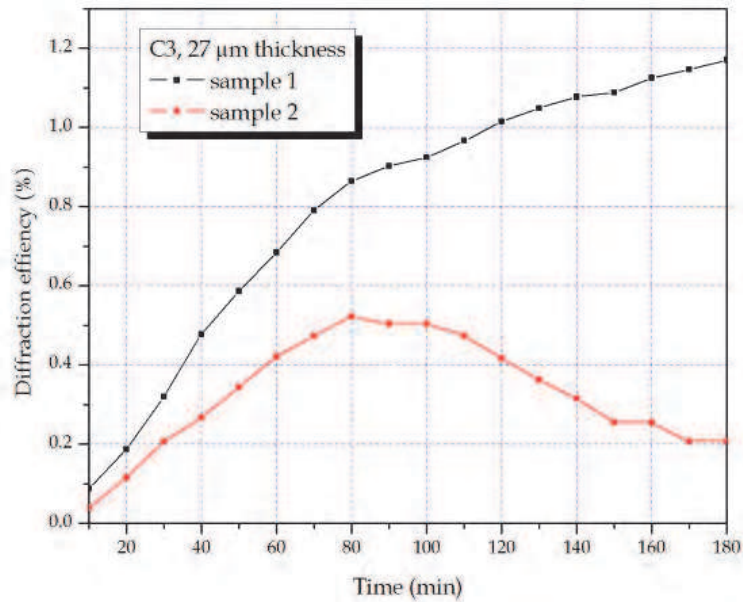


Fig. 16. (a). Plot of the Diffraction efficiency to certain temperature during the recording process.

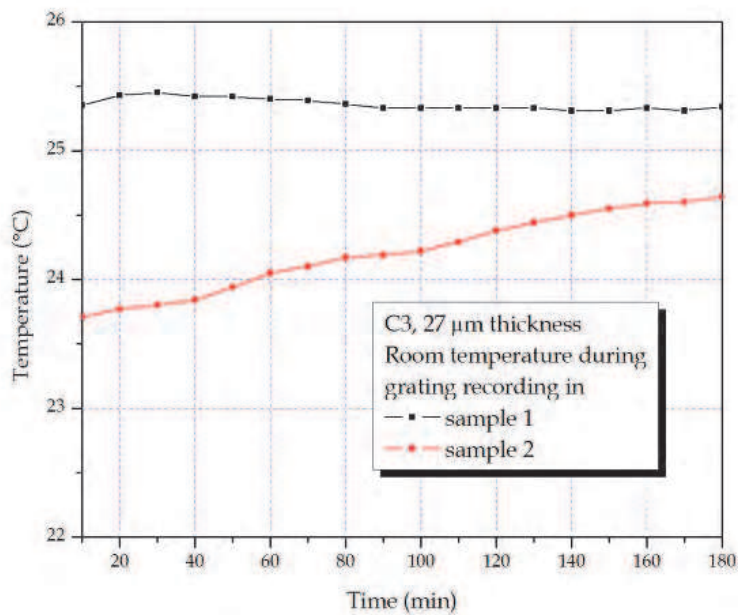


Fig. 16. (b). Temperature behavior during the recording process in the 27 μm thickness cell of two holographic gratings. The red and black line in both plots corresponds to same experiment.

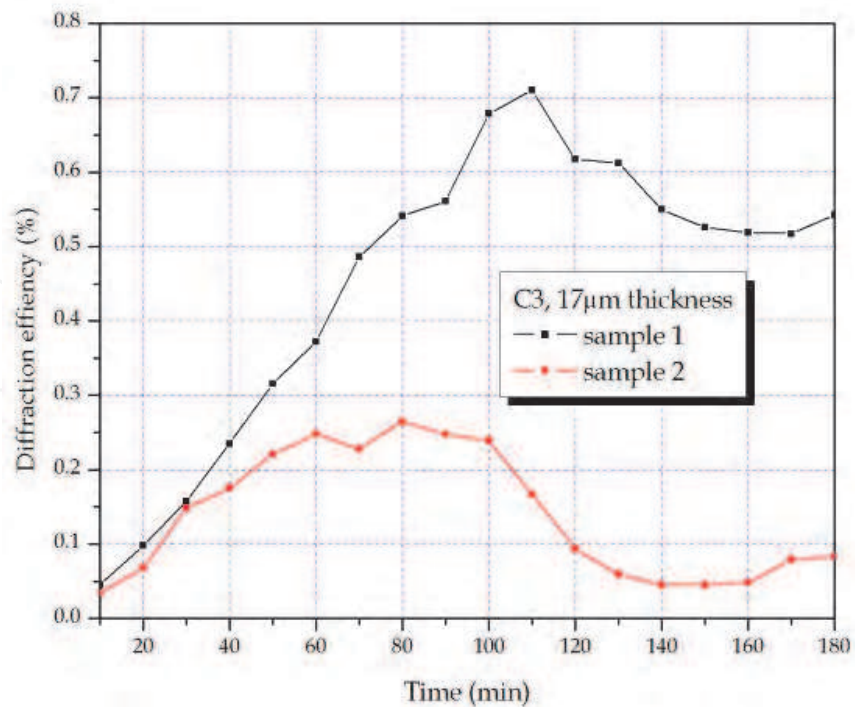


Fig. 17. (a). Plot of the Diffraction efficiency to certain temperature during the recording process.

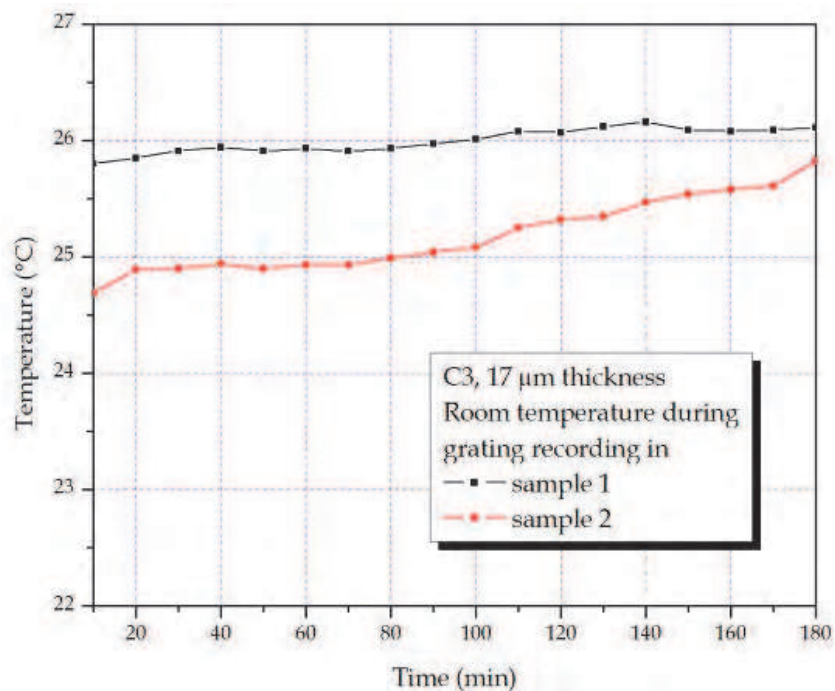


Fig. 17. (b). Temperature behavior during the recording process in the 17 μm thickness cell using the C3 concentration of two holographic gratings.

The temperature changes in the cases showed in Figs 15, 16, and 17 are due that we do not have temperature control in our laboratory. It is important to say; the gratings were recorded along different days. We can conclude that the temperature must be constant during the recording process about 25°C to obtain a softly behavior and the highest DE values.

5. Fourier holograms

Several types of holograms exist; these are of transmission, amplitude, phase, reflection, computer generated holograms, Fourier holograms, etc., (Smith, 1975).

A hologram can be done registering the interference pattern intensity between two beams, called a reference and an object beam, in a photosensitive material or holographic film as is shown in Fig. 18.

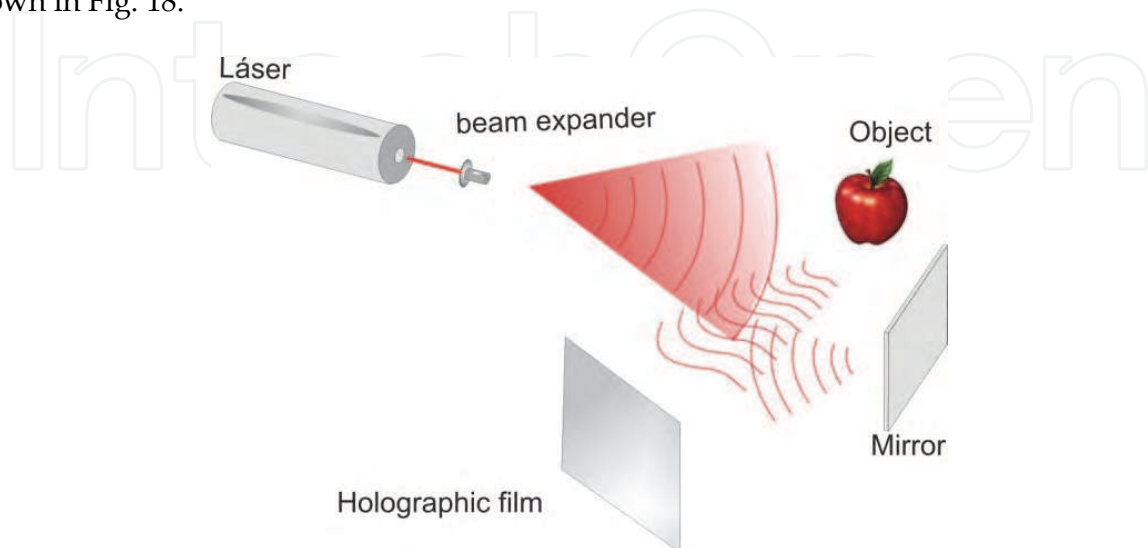


Fig. 18. Basic setup to hologram recording process, the beam reflected by the object is called object beam and the reflected beam by the mirror is the reference beam.

In particular, recording the interference pattern between the reference beam and the Fourier transform of an object produces the Fourier holograms. One of the main characteristics of this type of holograms is that the necessary area to record is small compared with other types of holograms. The Fig. 19 we depicted the scheme to record Fourier holograms.

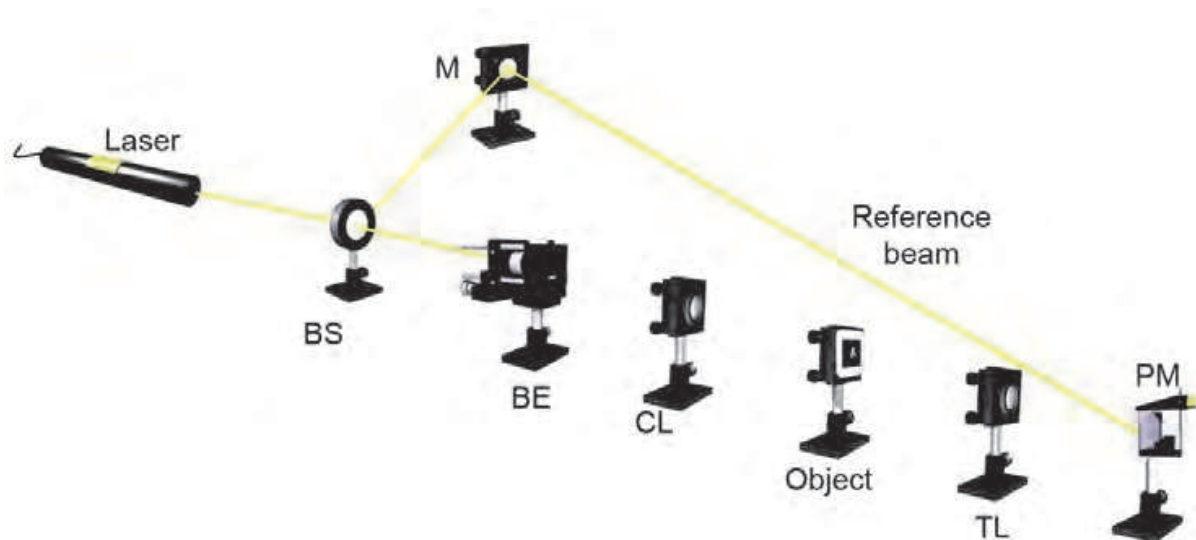


Fig. 19. Schematically representation for Fourier holograms recording. BS: beam splitter, BE beam expander, CL: Collimating lens, TL: transforming lens, PM: photosensitive material, M: mirror.

In the scheme of Fig. 19 a laser beam is expanded by microscope objective and a pinhole (BE) and collimated by the lens (CL) to produce a plane wave that illuminates the object $f(x, y)$; the converging lens (TL) obtains the Fourier transform of the object called object beam (O) and directs it into the photosensitive material (PM) where it interferes with the reference beam (R) coming from a mirror and the pattern is recorded.

Once the hologram was recorded, we use the same reference beam R to reconstruct the images as is depicted in Fig. 20. The reconstruction of the hologram produces two images, namely, real and conjugated images.

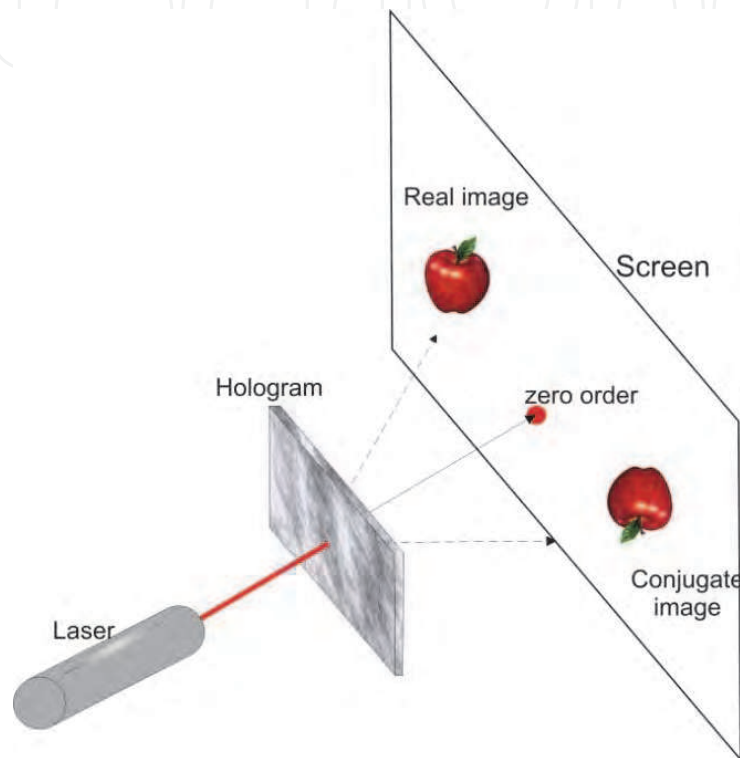


Fig. 20. Reconstruction of the real image of a hologram.

To explain mathematically the Fourier holograms we use the Fig. 21, where a point source is located at coordinates $x=-a$ and $y=0$. The divergent spherical beams is then transformed at plane wave for the lens and is used as the reference beam R, given by

$$R = R(x, y) = \frac{1}{\lambda f} \int_{-\infty}^{\infty} \int_{-\infty}^{\infty} \delta(x+a) \delta(y) e^{-i2\pi(vx+\mu y)} dx dy \quad (4)$$

where λ is the wavelength, f is the focal length of the lens, $v = x/\lambda f$ and $\mu = y/\lambda f$ are spatial frequencies. As is indicated in eq.*, the reference beam is a plane wave expressed by the Fourier transform of the point source $\delta(x+a) \delta(y)$ located at $x=-a$. Evaluating the integral in eq. (4), we can express the reference beam as:

$$R = A e^{i2\pi v a} \quad (5)$$

where A is the wave amplitude.

The object beam O is the Fourier transform of the object $f(x, y)$ and is given by

$$O = O(x, y) = \frac{1}{\lambda f} \int_{-\infty-\infty}^{\infty} \int_{-\infty-\infty}^{\infty} f(x, y) e^{-i2\pi(vx+\mu y)} dx dy \tag{6}$$

or

$$O = F\{f(x, y)\} \tag{7}$$

where the Fourier transform is denoted by F.

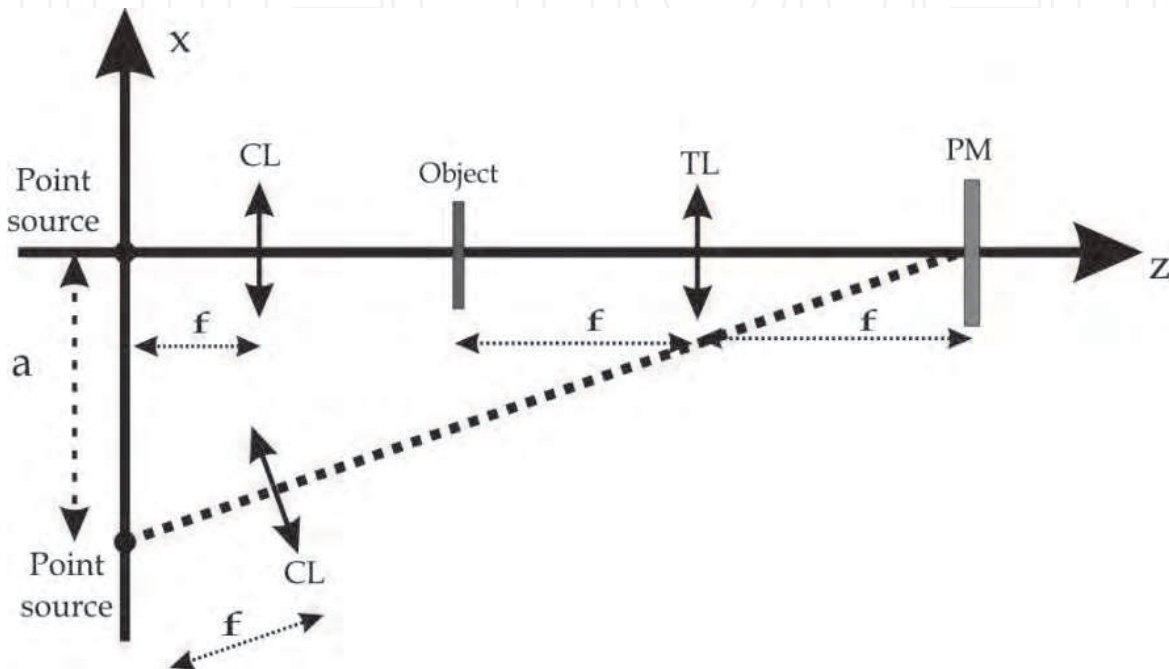


Fig. 21. Schematically representation of the Fourier holograms.

The photosensitive material, PM, registers the interference pattern intensity given by

$$I = |R + O|^2 \tag{8}$$

which can be expressed as

$$I = |R|^2 + |O|^2 + R^* O + R O^* \tag{9}$$

where the symbol * denotes the complex conjugate. Substituting the eqs. (5) and (7) in (9) we can obtain

$$I = A^2 + |F\{f(x, y)\}|^2 + A e^{-i2\pi va} F\{f(x, y)\} + A e^{i2\pi va} F^* \{f(x, y)\} \tag{10}$$

$$I = I_1 + I_2 + I_3 + I_4 \tag{11}$$

where

$$I_1 = A^2 \tag{12}$$

$$I_2 = |F\{f(x, y)\}|^2 \quad (13)$$

$$I_3 = Ae^{-i2\pi va} F\{f(x, y)\} \quad (14)$$

$$I_4 = Ae^{i2\pi va} F^*\{f(x, y)\} \quad (15)$$

In order to realize the reconstruction of the hologram, the reference beam R is used to illuminate the exposed film, so we can obtain

$$RI = RI_1 + RI_2 + RI_3 + RI_4 \quad (16)$$

The first two terms in right hand side of equation (15) are constants. The third term is expressed as

$$RI_3 = RAe^{-i2\pi va} F\{f(x, y)\} \quad (17)$$

and substituting eq. (5) in eq. (16) we obtain

$$RI_3 = A \int_{-\infty}^{\infty} \int_{-\infty}^{\infty} \delta(x+a)\delta(y) e^{-i2\pi(vx+\mu y)} e^{-i2\pi a} F\{f(x, y)\} dx dy \quad (18)$$

which can be reduced as

$$RI_3 = A \int_{-\infty}^{\infty} \int_{-\infty}^{\infty} F\{f(x+a, y)\} e^{-i2\pi(v(x+a)+\mu y)} dx dy \quad (19)$$

The result shown in eq. (18) can be interpreted as the double Fourier Transform of the object $f(x, y)$, i. e.

$$RI_3 = F\{F\{f(x+a, y)\}\} = Af(-x-a, -y) \quad (20)$$

where the Fourier transform properties was employed. This term is know as the real image of the object $f(x, y)$ located in the position $x=a$ and correspond to the +1 diffracted order. Similarly, developing the fourth term RI_4 we obtain

$$RI_4 = RAe^{i2\pi va} F^*\{f(x, y)\} \quad (21)$$

and substituting eq. (4) in eq. (21) and using the relation $F^*(f(x, y)) = -F(f^*(x, y))$ we obtain

$$RI_4 = -A \int_{-\infty}^{\infty} \int_{-\infty}^{\infty} \delta(x+a)\delta(y) e^{-i2\pi(vx+\mu y)} e^{i2\pi a} F^*\{f^*(x, y)\} dx dy \quad (22)$$

which can be reduced as

$$RI_4 = -A \int_{-\infty}^{\infty} \int_{-\infty}^{\infty} F\{f^*(x+a, y)\} e^{-i2\pi(v(x-a)+\mu y)} dx dy \quad (23)$$

Equation (22) can be reduced as following

$$RI_4 = -Af^*(-x-a,-y) \quad (24)$$

The term represented by eq. (23) is known as the conjugated image of the object $f(x, y)$ and is the -1 diffracted order.

According to above results, we use the concentration C3, the sample thickness 110 mm, intensity beams ratio 1:1 and 5 degrees between the interference beam to record Fourier holograms. In Fig. 19 we showed the representation of the setup employed, where we use a He-Ne laser at 594 nm wavelength as recording beam and a laser at 544 nm as reading beam. In Fig. 22 we show the exposed area in the cell and, as can be observed, this area is 1mm² approximately.

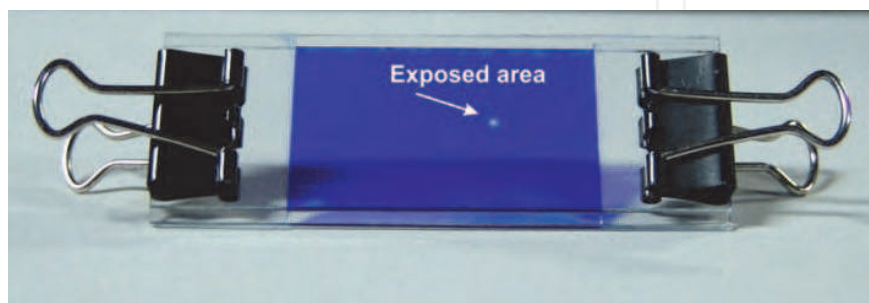


Fig. 22. Photography of the exposed area, the white point is the area where the Fourier hologram was recorded.

In Fig. 23 we show the two binary objects used to make Fourier holograms. The objects are the negative of the Universidad Michoacana de San Nicolás de Hidalgo logo and a text; the objects were photographed with a Nikon camera using a kodalith film and developed in a dark room following the Kodak instructions. After the objects were taken, we put it in the experimental setup and illuminates with a plane wave as is indicated in Fig 19. The reconstructed images are shown in Fig. 24 where only are the real images.

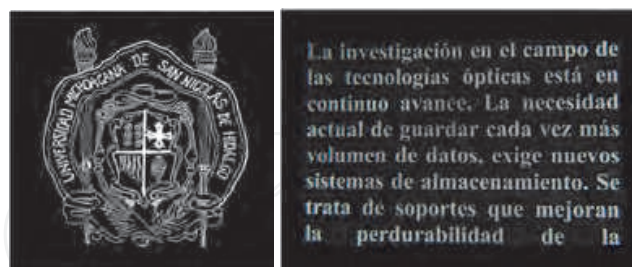


Fig. 23. Binary objects employed to Fourier holograms recording.



Fig. 24. Real images of the Fourier holograms recorded in our photosensitive material.

In order to compare our photosensitive material, we use the SO-253 film from Kodak to make the Fourier hologram of the text and the reconstructed real image is shown in Fig. 25. It is important to note, that the amount of text in Figs. 24 and 25 are different because we use 1 inch of diameter lens in one optical setup and 2 inch of diameter lens in the optical setup used in order to illuminate the photosensitive material. Another difference is that the SO-253 film has its sensibility at the line $\lambda=633$ nm so we record the Fourier hologram with this wavelength and we use the same wavelength to reconstruct the real image.

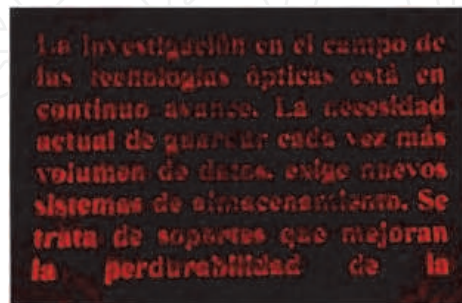


Fig. 25. Real image of hologram stored in SO 256 film from Kodak.

The advantage of Fourier holograms is that the storage area is small compared with Fresnel holograms and we can apply some multiplexing technique to optimizing the storage area. In table 6 we show the diffraction efficiencies of the holograms showed above measured for the +1-diffracted order.

| Hologram | Photosensitive material | Diffraction Efficiency (%) |
|---------------|-------------------------|----------------------------|
| UMSNH logo | NOA 65 and CV | 0.11 |
| Text hologram | NOA 65 and CV | 0.16 |
| Text hologram | SO-253 Kodak | 1.00 |

Table 6. Diffraction efficiencies for hologram reconstruction.

6. Conclusions

We present a photosensitive material composed by Norland Optical Adhesive No. 65[®] mixed with crystal violet dye with a high potential for recording holographic elements in real time, in this work we can emphasize some important characteristics of this material, eg: the phase holographic gratings are refraction index modulated, it is of low resolution; as is expected, a major sample thickness diffraction efficiency is increased, the beam intensity ratio must be 1:1 to obtain a best behavior of gratings. Also we noticed that the room temperature plays an essential role for the registry of holograms, that is to say, temperatures majors to 25 °C and minors to 24 °C its efficiency of diffraction are smaller, finally we have recorder Fourier holograms of binary objects in real time.

7. References

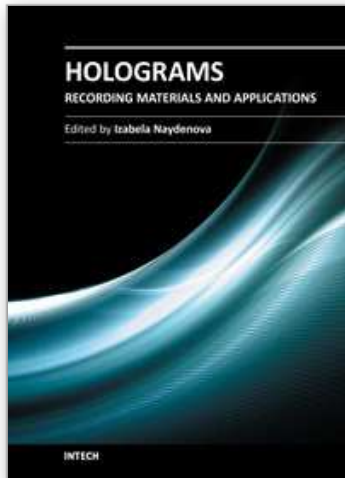
- Smith H. (1975). *Principles of holography*, second edition, Johnm Wiley & Sons.
- Bjelkhagen H., Thompson B. (1996). *Selected papers on holographic recording materials*, Vol. MS 130, SPIE Optical Engineering Press, Bellingham, USA.

- P. Hariharan, (1980). *Holographic recording materials: recent developments*, Optical Engineering, Vol. 19 (5), pp. 636-641.
- Kang D., Kim J. & Bae B. (2004). *Simple fabrication of diffraction gratings by two-beam interference method in highly photosensitive hybrid sol gel films*; Optics express, Vol. 12, No. 17, 3947-3953.
- Kostuk R. (1999). *Dynamic hologram recording characteristics in DuPont photopolymers*, Applied Optics, Vol. 38, No. 8, 1357-1363.
- Adhami R. Lanteigne, D. & Gregory D. (1991). *Photopolymer hologram formation theory*, Microwave and optical technology letters, Vol. 4, No. 3, 106-109.
- Gallego S., Ortuño M., Neipp C., Márquez A., Beléndez A., Pascual I., Kelly J. & Sheridan J. (2005). *3 Dimensional analysis of holographic photopolymers based memories*, Optics express, Vol. 13, No. 9, 3543-3557.
- Gleeson M., Kelly J., O'Neill F. & Sheridan J (2005). *Recording beam modulation during grating formation*, Applied Optics, Vol. 44, No. 26, 5475-5482.
- Neipp C., Gallego S, Ortuño M., Márquez A., Alvarez M., Beléndez A. & Pascual I. (2003). *First-harmonic diffusion-based model applied to a polyvinyl-alcohol-acrylamide-based photopolymer*, J. Opt. Soc. Am. B, Vol. 20, No. 10, 2052-2060.
- Ortuño M., Gallego S., Garcia C., Neipp C., Pascual I. (2003). *Holographic characteristics of a 1 mm-thick photopolymer to be used in holographic memories*, Applied Optics, Vol. 42, No. 35, 7008-7012.
- Luna D., Olivares A. & Barriel L. (1977). *Photoresist shipley 1350-J with crystal violet tint for holographic optical elements*, Optical Materials, 7, 189-195.
- Luna D., Olivares A., Barriel L. & Osorio F. (1998). *Rosin resin with crystal violet tint*, Optical materials 11, 95-100.
- Ortiz M., Alemán K., Pérez M. Ibarra J. C. & Olivares A. (2007). *Polyvinyl alcohol and crystal violet as photosensitive film*, SPIE, Vol. 6488.
- Fernández E., García C., Pascual I., Ortuño M., Gallego S. & Beléndez A. (2006). *Optimization of a thick polyvinyl alcohol-acrylamide photopolymer for data storage using a combination of angular and peristrophic holographic multiplexing*, Applied optics, Vol. 45, No. 29, 7661-7666.
- Martin S., Leclere P., Renotte Y., Toal V. & Lion Y. (1994). *Characterization of an acrylamide-based dry photopolymer holographic recording material*, Optical Engineering; Vol. 33, No. 12, 3942-3946.
- Naydenova I., Sherif H. , Mintova S, Martin S. & Toal V. (2006). *Holographic recording in nanoparticle-doped photopolymer*; Holography 2005, International Conference on Holography, Optical Recording and processing of Information, Proc. of SPIE Vol. 6252.
- Ibarra J. C. & Olivares A. (2002). *New holographic recording material: bromothymol blue dye with rosin*, Optical materials, Vol. 20, 73-80.
- Budinski K., M. K. Budinski (1999). *Engineering Materials Properties and Selection*, sixth ed., Prentice Hall, NJ.
- Pinto B., Olivares A. & Fuentes I. *Holographic material film composed by NOA 65[®] adhesive*; Optical Materials; 20 (2002); 225-232.
- Aleksejeva J. & Teteris J. (2010). *Volumen Grating Recording in Acrylate-Based Photopolymers*, Latvian Journal of Physics and Technical Sciences: Vol. 43 Number 3, pp 13-2. DOI: 10.2478/v10047-010-0010-5.

Norland Products Incorporated, Norland Optical Adhesive 65 (1996, 1999). 695 Joyce Kilmer Ave. New Brunswick, NJ (980) 545-7828 Catalog 0906-S01, 0906-S02.

IntechOpen

IntechOpen



Holograms - Recording Materials and Applications

Edited by Dr Izabela Naydenova

ISBN 978-953-307-981-3

Hard cover, 382 pages

Publisher InTech

Published online 09, November, 2011

Published in print edition November, 2011

Holograms - Recording Materials and Applications covers recent advances in the development of a broad range of holographic recording materials including ionic liquids in photopolymerisable materials, azo-dye containing materials, porous glass and polymer composites, amorphous chalcogenide films, Norland optical adhesive as holographic recording material and organic photochromic materials. In depth analysis of collinear holographic data storage and polychromatic reconstruction for volume holographic memory are included. Novel holographic devices, as well as application of holograms in security and signal processing are covered. Each chapter provides a comprehensive introduction to a specific topic, with a survey of developments to date.

How to reference

In order to correctly reference this scholarly work, feel free to copy and paste the following:

J.C. Ibarra, L. Aparicio-Ixta, M. Ortiz-Gutiérrez and C.R. Michel (2011). Norland Optical Adhesive 65® as Holographic Material, Holograms - Recording Materials and Applications, Dr Izabela Naydenova (Ed.), ISBN: 978-953-307-981-3, InTech, Available from: <http://www.intechopen.com/books/holograms-recording-materials-and-applications/norland-optical-adhesive-65-as-holographic-material>

INTECH
open science | open minds

InTech Europe

University Campus STeP Ri
Slavka Krautzeka 83/A
51000 Rijeka, Croatia
Phone: +385 (51) 770 447
Fax: +385 (51) 686 166
www.intechopen.com

InTech China

Unit 405, Office Block, Hotel Equatorial Shanghai
No.65, Yan An Road (West), Shanghai, 200040, China
中国上海市延安西路65号上海国际贵都大饭店办公楼405单元
Phone: +86-21-62489820
Fax: +86-21-62489821

© 2011 The Author(s). Licensee IntechOpen. This is an open access article distributed under the terms of the [Creative Commons Attribution 3.0 License](#), which permits unrestricted use, distribution, and reproduction in any medium, provided the original work is properly cited.

IntechOpen

IntechOpen